Published in final edited form as:
Nat Cell Biol. 2005 June ; 7(6): 559–569.

Caenorhabditis elegans RME-6, a novel regulator of Rab5 at the clathrin-coated pit

Miyuki Sato[1], **Ken Sato**[1,3], **Paul Fonarev**[1], **Chih-Jen Huang**[2], **Willisa Liou**[2], and **Barth D. Grant**[1,4]

1 *Department of Molecular Biology and Biochemistry, Rutgers University, Piscataway, NJ 08854, USA*

2 *Department of Anatomy, Chang Gung University, Kwei-Shan Tao-Yuan, Taiwan, 333, R.O.C*

3 *Molecular Membrane Biology Laboratory, RIKEN, Wako, Saitama 351-0198, Japan*

Abstract

Using *C. elegans* genetics we identified a new regulator of endocytosis called RME-6. RME-6 is evolutionarily conserved among metazoans and contains RasGAP-like and Vsp9 domains. Consistent with the known catalytic function of Vps9 domains in Rab5 GDP/GTP exchange, we found that RME-6 binds specifically to *C. elegans* Rab5 in the GDP-bound conformation, and *rme-6* mutants display phenotypes that indicate low Rab5 activity. Furthermore, *rme-6* interacts genetically with the worm homologue of the known Rab5 exchange factor Rabex-5. However, unlike other Rab5 associated proteins, a rescuing GFP::RME-6 fusion protein primarily localizes to clathrin-coated pits, physically interacts with α-adaptin, a clathrin adaptor protein, and requires clathrin to achieve its cortical localization. In *rme-6* mutants transport from the plasma membrane to endosomes is defective, and small 100 nm endocytic vesicles accumulate just below the plasma membrane. These results suggest a mechanism for the activation of Rab5 in clathrin-coated pits or clathrin coated vesicles that is essential for the delivery of endocytic cargo to early endosomes.

Introduction

Clathrin-dependent endocytosis is the major route by which most receptor-ligand complexes are internalized. Clathrin and cargo molecules are assembled into clathrin-coated pits on the plasma membrane (PM) together with adaptor proteins that link clathrin and transmembrane receptors, concluding in the formation of mature clathrin-coated vesicles (CCVs). CCVs are then actively uncoated and transported to early/sorting endosomes[1]. These processes are highly regulated but the precise molecular mechanisms controlling these steps are not fully understood.

Small GTPases of the Rab family play pivotal roles in vesicular transport[2]. Rab5 in particular is known as a key regulator of the early endocytic pathway. Rab5 is found associated with the PM, CCVs, and most prominently with early endosomes[3,4]. Rab5 is thought to regulate homotypic fusion of early endosomes, microtubule-based motility of early endosomes, and the organization of subdomains within the early endosome limiting membrane, through its ordered recruitment of multiple effectors to the endosomal periphery[5–8]. *In vitro* studies also indicate that Rab5 regulates heterotypic fusion of CCVs with early endosomes, and in complex with GDI, Rab5 has been proposed to function in ligand sequestration during clathrin-coated pit formation[9–11].

4 Correspondence:grant@biology.rutgers.edu.

To exert such diverse functions, the activity of Rab5 must be spatially and temporally controlled, probably at the level of nucleotide exchange by guanine nucleotide exchange factors (GEFs). Rabex-5 is the canonical Rab5 GEF and is essential for Rab5-dependent fusion of early endosomes *in vitro*[9]. Studies on the catalytic function of Rabex-5 revealed that the conserved Vps9 domain is necessary and sufficient for the observed enhancement of Rab5 GDP/GTP exchange rates by Rabex-5[12]. In mammals, Rab5 GEF activity has also been biochemically demonstrated for two other Vps9-domain proteins, RIN1 and Alsin, suggesting that Rab5 is regulated by multiple GEFs *in vivo*[13,14]. Rab5 GEF activity associated with clathrin-coated vesicles has also been identified *in vitro*, but the particular protein that confers this activity remains to be determined[15].

Here we report molecular cloning and functional characterization of RME-6, an evolutionarily conserved protein containing both RasGAP-related and Vps9 domains. Our results demonstrate that RME-6 is a key new regulator of RAB-5 required for endocytosis from the PM.

Results

rme-6 mutants display endocytosis defects in oocytes and coelomocytes

We isolated four alleles of *rme-6* in a previously reported genetic screen for mutants defective in oocyte endocytosis of YP170::GFP, a reporter for clathrin-dependent endocytosis in C. elegans[16]. In these *rme-6* mutants, YP170-uptake by oocytes was strongly reduced, resulting in accumulation of YP170::GFP in the body cavity and very little YP170::GFP in oocytes (RME phenotype; Fig.1 d). Seven alleles of *rme-6* were also identified in a different genetic screen for coelomocyte endocytosis mutants (Fig. 1e)[17]. As shown in Fig. 1f, *rme-6* mutants exhibit a high level accumulation of a fluid-phase endocytosis marker (GFP secreted by muscle) in the body cavity, indicating a severe defect in endocytosis by coelomocytes. These phenotypes in oocytes and coelomocytes suggest that *rme-6* is generally required for endocytosis in multiple tissues.

rme-6 encodes a conserved protein with RasGap-like and Vps9 domains

We cloned the wild-type *rme-6* gene using standard methods and identified sequence changes associated with each of the *rme-6* alleles (Fig. 1g and Supplemental figure S1; see materials and methods). The *rme-6* gene encodes a novel 1093 amino acid protein (Fig. 1g). The most notable feature of the predicted RME-6 sequence is a Vps9 domain at the C-terminus, a motif found in the catalytic domains of Rab5 GEFs including human Rabex-5, RIN1, and yeast Vps9p[12]. In addition to the Vps9 domain, RME-6 contains a RasGAP-related domain in the N-terminal region[18]. We found predicted fly and mammalian homologues of RME-6 in genome databases, and the overall domain structure is well conserved among them. The *C. elegans* genome has a homologue of Rabex-5, the canonical Rab5 GEF, which is encoded by Y39A1A.5/*rabx-5* on chromosome III. Human and worm Rabex-5 proteins display a characteristic domain structure including an N-terminal zinc finger domain and a central Vps9 domain. RME-6 and Rabex-5 share sequence similarity only within a limited region comprised primarily of the Vps9 domain (Supplemental figure S1). Thus, RME-6 is a new Vps9-domain containing protein conserved from worm to human (Fig.1h).

The N-terminal RasGap-like sequence is highly conserved among RME-6 proteins, implying an important function for this domain (Supplemental figure S1). Similar GAP-related domains are found in the family of GTPase activating proteins (GAP) specific for Ras, such as human p120GAP and *C. elegans* GAP-1 and GAP-2[18–20]. This motif is also found in IQGAP proteins, which lack GAP activity toward Ras but are known to instead interact with Rac and Cdc42[21]. Interestingly, this domain within IQGAP1 shows the highest similarity with the RME-6 N-terminus (Supplemental figure S1).

We detected a protein of the predicted size for RME-6 (130 kDa) in wild-type worm lysates by immunoblotting using an affinity purified anti-RME-6 antibody that we developed (Fig.1i). The 130 kDa band is missing from *rme-6(b1014)* null mutant lysates.

RME-6 physically interacts with a predicted GDP-bound form of RAB-5

Rab5 is known as the key regulator of early endocytic events in mammalian systems[4,6]. We have also previously demonstrated that RAB-5 is required for endocytosis in *C. elegans*[16]. The existence of the Vps9 domain in RME-6 led us to speculate that RME-6 regulates endocytosis through activation of RAB-5. To test this hypothesis, we first examined physical interaction between RME-6 and RAB-5 using yeast two-hybrid analysis (Fig. 2a). Similar to previously reported results for known Rab5 exchange factors[13,22], RME-6 specifically interacted with RAB-5(S33N), which is a mutant form of RAB-5 expected to be locked in the GDP-bound conformation. No interaction was detected with the wild-type or GTPase defective mutant RAB-5(Q78L) in this assay. Moreover, this interaction was specific for RAB-5 because RME-6 showed no interaction with RAB-7 or its mutant forms.

Physical interaction between RME-6 and RAB-5 was further confirmed by co-immunoprecipitation analysis in transfected COS cells. GFP or a fusion of GFP and C.e. RME-6 were co-expressed in COS-7 cells together with HA-tagged C.e. RAB-5 or its mutant forms. HA-RAB-5 was immunoprecipitated from total cell lysates using an anti-HA antibody. Precipitants were probed with anti-GFP antibody on Western blots (Fig. 2b). We observed significant co-immunoprecipitation of GFP::RME-6 with all three forms of HA-RAB-5. Consistent with the result of the two-hybrid assay, by far the strongest interaction we observed was between GFP::RME-6 and HA-RAB5(S33N), even though the HA-RAB-5(S33N) mutant expressed poorly in COS cells compared to the other HA-RAB-5 forms. No interaction was detected between GFP alone and any form of HA-RAB-5, indicating the specificity of the interaction. The preferential interaction of RME-6 with the GDP-bound RAB-5 in two different assays strongly suggests that RME-6 functions as a GEF for RAB-5.

RME-6 and C.e. Rabex-5 are partially redundant for membrane localization of RAB-5 and animal viability

The phenotypes we have described here for *rme-6* mutants are very similar to those we have previously described for *rab-5*(RNAi), except that loss of *rab-5* activity is lethal, while loss of RME-6 is not[16]. We speculated that this difference might result from residual RAB-5 activation in *rme-6* mutants mediated by RABX-5, the apparent worm orthologue of Rabex-5[9]. In mammalian systems, Rabex-5 is found in a stable complex with Rabaptin-5, a Rab5 effector protein[9,23]. It has been proposed that Rabex-5 and Rabaptin-5 require one-another for function. The *C. elegans* genome contains a putative worm Rabaptin-5, F01F1.4/*rabn-5*. And indeed we found that worm RABX-5 can interact with the putative worm Rab-5 effector RABN-5 as well as GDP-bound RAB-5 in yeast two-hybrid assays (Supplementary figure S2). These results suggest that a functional Rabex-5-Rabaptin-5 complex exists in worms, similar to the well-studied complex in mammals.

Surprisingly, neither *rabx-5*(RNAi) nor *rabn-5*(RNAi) had significant effects on YP170::GFP endocytosis by oocytes, ssGFP endocytosis by coelomocytes, or on animal viability (Fig. 3e; data not shown). We also observed normal YP170::GFP endocytosis by oocytes in a *rabx-5 (tm1512)* mutant that lacks RABX-5 protein as assayed by immunoblotting (Supplemental fig. S2).

Unlike either single mutant however, RNAi of *rabx-5* or *rabn-5* in an *rme-6(b1014)* mutant background resulted in strong synthetic lethality (Fig. 3e). Many of the arrested larvae displayed a molting defect, a phenotype often associated with worms severely compromised

for endocytic function[24,25]. These synthetic phenotypes indicate a partial redundancy between RME-6 and the RABX-5-RABN-5 complex for endocytic function.

If RME-6 functions as a RAB-5 GEF we would expect to observe phenotypic effects in *rme-6* mutants that reflect low RAB-5 activation. In an effort to identify such defects we examined the effect of *rme-6* mutations and/or *rabx-5* mutations or RNAi on the subcellular localization of GFP::RAB-5 expressed in oocytes. In wild-type oocytes, GFP::RAB-5 is mainly localized to endosomes with a punctate appearance in the cortex (Fig. 3a). In *rme-6(b1014)*, the size of these GFP::RAB-5-positive structures was reduced by an average of about 3-fold (Fig. 3 b and f). This phenotype is consistent with decreased membrane influx into endosomes or a defect in homotypic endosome fusion. Mutation or RNAi of *rabx-5* produced a similar reduction in the size of GFP::RAB-5 positive endosomes, but did not affect YP170::GFP endocytosis *per se*, consistent with a defect in homotypic endosome fusion (Fig. 3c and f). Strikingly, the punctate pattern of GFP::RAB-5 completely disappeared in *rme-6(b1014)* mutants depleted of *rabx-5* by RNAi (Fig. 3d). Instead, in oocytes lacking RME-6 and RABX-5, GFP::RAB-5 appeared diffuse in the cytoplasm. We confirmed that the GFP::RAB-5 protein levels were not affected by the mutations or RNAi's by anti-GFP immunoblotting (Fig. 3e). Taken together these results indicate that RAB-5 function is severely impaired in *rme-6* mutants, and that the all or most of the residual RAB-5 activity in *rme-6* mutants is mediated by RABX-5.

A very early step of endocytosis is blocked in *rme-6* mutants.

In order to better understand which step of endocytosis is impaired in *rme-6* mutants, we performed pulse-chase analysis of endocytosis in coelomocyte cells using a previously established assay[24]. In this assay, trafficking of Texas Red-labeled BSA (TR-BSA) microinjected into the body cavity was followed as a function of time. To better visualize endosomes during endocytosis, our analysis was performed in transgenic animals expressing the endosome marker RME-8::GFP[24]. In wild-type, we first observed TR-BSA in the RME-8::GFP-positive endosomes 5 to 10 min after injection of the tracer into the body cavity (Fig. 4a, arrow heads). By 30 min after injection, TR-BSA began to leave the endosomes and accumulate within RME-8::GFP negative lysosomes (Fig. 4a, arrows). In *rme-6(b1014)* mutants, the earliest visible accumulation of TR-BSA in coelomocytes was abnormal and greatly retarded. At early time points, TR-BSA was often observed as a weak signal in an RME-8 negative region of the coelomocyte, very close to the PM (Fig. 4b, large arrows). Because internalization of TR-BSA into coelomocytes is a vesicle-mediated process, we assume that this diffuse TR-BSA signal represents clusters of small vesicles that have accumulated in *rme-6* mutant coelomocytes. Concentration of TR-BSA within RME-8::GFP labeled endosomes became visible 30 to 60 min after injection (Fig. 4b, arrow heads). TR-BSA finally reached the terminal compartment of the coelomocytes 60–120 min after injection. These results suggest that the primary defect in *rme-6* mutants is during a very early step of endocytosis.

We also sought further evidence to define the primary defect in *rme-6* mutant oocytes. To do this we determined the distribution of the yolk receptor, RME-2[16], in oocytes by immunoelectron microscopy (Fig. 5). Since RME-2 constantly cycles between the PM and endosomes, most RME-2 in wild-type oocytes at steady-state is found in cortical endocytic membrane structures (Fig. 5a). We detected RME-2 mainly in two types of vesicles in wildtype. One class of vesicles showed variable size that ranged from 120 to 250 nm and probably represent early or sorting endosomes (Fig. 5a small arrows). The second class of vesicles are very small, less than 50 nm in diameter and appear to be cross-sectional views of tubulo-vesicular structures, probably recycling endosomes (Fig. 5a large arrows).

Strikingly, in *rme-6(b1014)*, most yolk receptors accumulate very near the PM in clusters of vesicles that may be docked with one-another (Fig. 5 b–d; arrow heads in panel b). The diameter of these vesicles was quite uniform at approximately 100 nm, very close to the known size of CCVs in other systems. In wild-type oocytes, clusters of such vesicles were never observed. We found that, in the *rme-6* mutant, 38% of total gold particles were detected associated with these clusters of small vesicles less than 120 nm in diameter, and only 6% of particles were found on endocytic structures larger than 120 nm (Fig. 5e). In wildtype, RME-2 was almost equally distributed among small and large endocytic vesicles (Fig. 5e). We consider it likely that the accumulated clusters of vesicles in *rme-6* mutants are intermediates of PM to early endosome transport and may be uncoated primary endocytic vesicles. Combined with the defects we observed in pulse-chase experiments in coelomocytes, these results indicate a very early role for RME-6 in endocytosis.

GFP::RME-6 colocalizes with clathrin-coated pit markers

In order to better understand the function of RME-6 in endocytosis, we determined its subcellular localization. Toward this end we created transgenic worms expressing either GFP::RME-6 or RME-6::GFP fusion proteins, each under the control of the *rme-6* promoter. Expression of these RME-6 fusion proteins fully rescues the coelomocyte endocytosis defect of *rme-6(b1014)*, indicating that GFP::RME-6 is functional and is very likely to be correctly localized (Supplemental fig. S3). GFP::RME-6 was expressed in many tissues (Fig. 6 a–d, data not shown). Interestingly, in intestinal and pharyngeal cells, GFP::RME-6 was clearly concentrated on the PM. In coelomocytes, GFP::RME-6 was also localized on or very close to the PM.

To define the subcellular localization of RME-6 we first performed double labeling of GFP::RME-6 and mRFP::RME-6 with endocytic compartment markers in coelomocytes. In particular we focused on two markers for PM clathin-coated pits: clathrin heavy chain (CHC-1) and α-adaptin (APT-4), and two markers for early endosomes: EEA-1 and RAB-5 in coelomocytes (Fig. 7 b-d and Supplemental fig. S4a).

Most GFP::RME-6 did not overlap with mRFP1::EEA-1 or mRFP1::RAB-5. In contrast, we found strong colocalization of GFP::RME-6 with mRFP1::CHC-1 and mRFP1::α-adaptin on or near the PM of coelomocytes. Interestingly, mRFP1::CHC-1 and mRFP1::α-adaptin as well as GFP::RME-6 were distributed unevenly around the PM, with regions of high and low labeling, reminiscent of the uneven distribution of endocytic pit structures that can be seen in coleomocytes by EM[26]. We observed similar colocalization with mRFP::RME-6 and GFP::CHC-1, a tagged form of worm CHC-1 that has been extensively studied before[25] (Fig. 7a). These results indicated that most RME-6 is associated with clathrin-coated pits and that only a minor fraction of the RME-6 in the cells is associated with early endosomes.

We made similar observations of GFP::RME-6 subcellular localization in oocytes and the hypodermis. To analyze RME-6 distribution in oocytes, we established strains expressing GFP::RME-6 in the *rme-6(b1014)* background under *pie-1* promoter control[27,28]. Expression of GFP::RME-6 in oocytes completely rescued the yolk endocytosis defect of the *rme-6 (b1014)* null mutant. We found that GFP::RME-6 was concentrated on small puncta, which were on or close to the PM of oocytes (Fig. 6 e and f). We observed strong colocalization of this GFP::RME-6 with mRFP1::CHC-1 surface puncta indicating that RME-6 labels coated pits or vesicles (Fig. 7e). On the other hand, GFP::RME-6 in oocytes showed little spatial overlap with endogenous EEA-1 as assayed using a previously published anti-EEA-1 antibody[43,45](Supplemental fig. S4b). Clear colocalization of GFP::RME-6 and mRFP::CHC-1 was also evident in hypodermal cells (Fig. 7f). We noted that RME-6 and coated pit marker colocalization was not perfect and that the ratio of intensities of GFP::RME-6 and mRFP1::CHC-1 varied from puncta to puncta, implying that GFP::RME-6 may associate with

clathrin-coated pits at a specific stage in their formation. This colocalization of GFP::RME-6 with clathrin-coated pit markers suggests that the primary function of RME-6 is to activate RAB-5 on the plasma membrane and in coated pits, a location where mammalian Rab5 is found and has been suggested to function, but for which a Rab5 activation mechanism has remained obscure.

Clathrin is required for the cell surface localization of GFP::RME-6

If RME-6 is localized by association with clathrin-coated pits, then we would expect that removal of these structures would disrupt RME-6 localization. Indeed, we found that RNAi-mediated knockdown of CHC-1, but not RAB-5 disrupts the cortical localization of GFP::RME-6 in oocytes (Fig. 8 a–d). Under the conditions used, RNAi of either *chc-1* or *rab-5* blocked yolk-uptake and resulted in embryonic lethality, indicating that the RNAi-mediated depletions worked efficiently. In *chc-1*(RNAi) animals, cortical GFP::RME-6 in oocytes disappeared almost completely (27/30 animals assayed). Thus the cortical localization of GFP::RME-6 depends upon clathrin. RNAi of *rab-5* did not reduce the cortical localization of GFP::RME-6, but in many animals the GFP::RME-6 cortical localization appeared more concentrated compared to control worms. RNAi treatment using *rab-7* or non-specific DNA fragments showed no obvious effect on GFP::RME-6 localization (data not shown).

RME-6 interacts physically with a clathrin adaptor protein

These results suggest a physical interaction between RME-6 and clathrin-coated pit components *in vivo*. To test this possibility we performed co-immunoprecipitation experiments between GFP-tagged RME-6 and endogenous α-adaptin from whole worm lysates (Fig. 8e and f). We found that α-adaptin did indeed coimmunoprecipitate with GFP::RME-6, showing a physical link of RME-6 to clathrin-coated pits.

Discussion

Here we demonstrate the existence and *in vivo* relevance of a key new Rab5 regulator closely associated with the clathrin-coated pit. In mammalian systems, Rab5 is known as a rate-limiting regulator of early endocytic events[4]. Rab5 is found on the PM and in coated-pits as well as on early endosomes[3,4]. Overexpression of a dominant-negative form of Rab5 inhibits uptake of endocytic cargo into cells[4,29] and causes accumulation of cargo in coated-pits[30]. Despite this mounting evidence for Rab5 function in coated-pit mediated internalization, most known Rab5-associated proteins localize to and function in early endosomes, and the functional importance and activation mechanism for Rab5 in coated-pits has remained obscure[5,6,23,31].

Our detailed phenotypic analyses and the coated-pit association of RME-6 presented here indicate a primary function for RME-6 in activating RAB-5 in clathrin-coated pits and/or primary endocytic vesicles. In particular, we found by immunoEM that in the absence of RME-6 function, oocyte cells accumulate clusters of 100 nm vesicles containing receptors, suggesting that fusion of endocytic vesicles with one-another and with early endosomes is severely impaired. Consistent with previous analysis of Rab5 function *in vitro*[11], *rme-6* mutants do not show any obvious defects in coated-pit size or number (data not shown), suggesting that the formation of clathrin-coated pits *per se* does not require RME-6 or Rab5.

In vitro fusion assays of CCVs and early endosomes indicate that Rab5 is necessary on both donor and target membranes[10]. However, EEA1 and hVps34, known Rab5 effectors involved in early endosome fusion are absent from CCVs[10]. Such asymmetric localization of downstream effectors has been proposed to be important for directional transport. How can asymmetric recruitment of Rab5 effectors to CCVs or early endosomes be achieved? One

possibility is that activation of Rab5 by different GEFs is coupled with recruitment of a distinct set of downstream Rab5 effectors. CCVs have been reported to possess Rab5 GEF activity, although the molecular nature of this activity has not been elucidated[15]. Our results suggest that RME-6 is such an activator of RAB-5 on clathrin-coated pits and/or CCVs and could be the activity detected previously by others.

The coated-pit association of RME-6 suggests that RAB-5 is recruited and activated before or during coated-vesicle formation. It has been shown that the Rab5-GDI complex enhances sequestration of cargo into clathrin-coated pits *in vitro,* and that GDP-GTP exchange of Rab5 is necessary for this activity[11]. RME-6 may be involved in cargo selection at the PM, although it is difficult to directly address this issue in the *C. elegans* system. Alternatively, Rab5 may be recruited before vesicle formation to ensure formation of fusion-competent vesicles. This second model would best explain the phenotypes we observed in *rme-6* mutants. The reduction in endosome size without an obvious reduction in overall endocytic transport in *rabx-5* mutants or RNAi treated animals is most consistent with a role for *rabx-5* in homotypic endosome fusion, and may indicate that homotypic endosome fusion is not strictly required for endocytosis *per se*. It is also interesting to note that others have found that Rabaptin-5 in complex with Rabex-5 binds to γ-adaptin and GGA1, clathrin adaptor molecules involved in TGN to endosome transport[32,33]. Thus recruitment of Rab5 GEFs to donor vesicles by interaction with coat proteins could be a general mechanism for activation of Rab5 on vesicles that ensures subsequent fusion with acceptor membranes.

The physical interaction that we demonstrated between RME-6 and α-adaptin could be direct or mediated by bridging proteins and awaits further analysis. We note however that within the Vps9 domain of RME-6 there is a sequence similar to a known α-adaptin ear binding motif, WxxF (RME-6; 1079WVNF)[34].

Rabex-5 forms a stable complex with Rabaptin-5, one of the known Rab5 effectors, and also exists as part of a large oligomeric EEA1 positive complex on early endosomes[6,9]. Interestingly, RME-6 appears not to interact with *C. elegans* Rabaptin-5 (RABN-5) in two-hybrid assays (our unpublished result) or with EEA-1 in coimmunoprecipitation assays (Fig. 8e). These results support the idea that RME-6 and Rabex-5-dependent activation of Rab5 are responsible for regulation of different sets of downstream effectors. The fact that loss of RME-6 or RABX-5 alone results in reduced endosome size, but only loss of RME-6 impairs ligand uptake by endocytosis further supports the idea that RME-6 has a primary function in uptake from the plasma membrane while RABX-5 probably functions primarily in homotypic endosome fusion. However, the synthetic phenotypes we uncovered when worms lack both *rme-6* and *rabx-5* activity indicate that when *rme-6* is missing *rabx-5* can partially substitute at the plasma membrane.

In addition to the Vps9 domain, RME-6 family members have a RasGAP-related domain near their N-termini that may modulate RME-6 function in response to a signaling pathway and/or may function to send signals derived from RAB-5. Our preliminary analysis has failed to identify genetic or physical interactions between RME-6 and LET-60, the canonical *C. elegans* Ras[35]. We deem it likely that RME-6 instead interacts with another member of the Ras family, or that it interacts with a Rho-family GTPase as in the case for IQGAP1, another protein with a RasGAP-like domain[21]. To elucidate the precise function of RME-6 and Rab5 in coated-pits and to identify putative effectors involved in this process, it will be important to determine the function of the N-terminal domain of RME-6 and identify additional proteins that function with RME-6 in endocytosis.

Materials and Methods

General methods and strains

C. elegans strains were derived from the wild-type Bristol strain N2. Worm cultures, genetic crosses, and other *C. elegans* methods were performed according to standard protocols[36]. Strains expressing transgenes in germline cells were grown at 25°C. Other strains were grown at 20°C. Transgenic strain *bIs1* [*vit-2::GFP*] expressing a fusion of YP170, a yolk protein, and GFP was used to monitor yolk uptake by oocytes[16]. Coelomocyte endocytosis was assayed using *arIs37* [p*myo-3::ssGFP*] or *cdIs5* [p*myo-3::ssDsRed2*][17,37] A deletion allele of *rabx-5* (*tm1512*) was provided by Shohei Mitani of the Japanese National Bioresource Project for nematodes. This mutant lacks 983 bp of the *rabx-5* gene including the second exon and a part of the third exon (nucleotides 8810/8811-9793/9794 in the cosmid Y39A1A), which deletes part of the coding region, is expected to cause a frameshift placing all downstream coding regions, including the catalytic vps9 domain, out of frame. This mutation was followed through genetic crosses by PCR using primers, rabx5-F (5′-ATTCCCCCAGATTGTGTATG-3′) and rabx5-R (5′-CCGGTGACGTGGAAGTTGGT-3′). Transgenic strains constructed for this study are; *pwIs2* [*GFP::rme-6*]; *pwIs169* [p*pie-1::GFP::rme-6*]; *pwIs20* [p*pie-1::GFP::rab-5*]; *pwIs53* [p*pie-1::mRFP::chc-1*]; *pwIs31* [p*unc-122::GFP::rme-6*]; *pwIs167* [p*unc-122::mRFP::chc-1*]; *pwIs177* [p*unc-122::mRFP::apt-4*]; *pwIs179* [p*unc-122::mRFP::eea-1*]; *pwEx81* [p*unc-122::mRFP::rme-6; GFP::CHC*]; *pwEx82* [*rme-6::GFP*]. *bIs34* [*rme-8::GFP*] and *bIs5* [*GFP::CHC*] were described previously [24,25].

RNA interference (RNAi) was performed by the feeding method[38]. cDNAs were prepared from EST clone provided by Yuji Kohara (National Institute of Genetics, Japan) and subcloned into RNAi vector L4440[39]. For RNAi knockdown L4 worms were placed onto RNAi plates, and P0 adults (after 24 hours) or F1 progeny (after 3 to 4 days) were subsequently scored for phenotype.

Genetic mapping and molecular cloning

b1014, *b1015*, *b1018*, and *b1019ts* were isolated in a screen described previously[16]. Briefly, *bIs1* [*vit-2::GFP*] was mutagenized with EMS or ENU, and the F2 generation was screened for animals exhibiting little or no GFP signal in oocytes and embryos but showing bright GFP signal in the body cavity. *ar471*, *ar474*, *ar476*, *ar477*, *ar483*, *ar507* and *ar511* were identified in unrelated screening for coelomocyte endocytosis-defective mutants and generously provided to us by Hanna Fares and Iva Greenwald[17]. All *rme-6* mutations are recessive and most of them show constitutive endocytosis defects at all temperature tested. Only *b1019* displays a temperature-sensitive defect in YP170::GFP endocytosis by oocytes. *rme-6* mutant worms also display slow growth and small body size at all temperatures, and a low brood size at 25°C (N2, 204±23; *rme-6(b1014)*, 67±11).

The *rme-6* mutations were mapped to the left-hand of LGX by sequence-tagged site polymorphism mapping[40]. Tight linkage between *rme-6* and *unc-1* was shown by the following three-point mapping results; *egl-17* (11/11) *rme-6* (0/11) *unc-1*; and *unc-1* (0/53) *rme-6* (53/53) *dpy-3*. The map position of *rme-6* was further refined by complementation test with deficiencies; meDf6 failed to complement *rme-6* but meDf2, meDf3 and meDf5 complemented. To identify a candidate for *rme-6*, we surveyed predicted genes in the *C. elegans* genomic sequence in this region by RNAi for the RME phenotype. RNAi for one of these genes, F49E7.1a, which encodes a protein with the Vps9 domain, produced a strong RME phenotype similar to *rme-6* mutants. Rescue of the coelomocyte endocytosis defect of an *rme-6 (b1018); arIs37* strain was achieved by microinjection of a 7.2kb PCR amplified DNA fragment including the complete F49E7.1a gene (at 10 μg/ml) together with the dominant

transgenic marker *rol-6(su1006)* (pRF4, 100μg/ml). All exons from F49E7.1a were amplified from each *rme-6* mutant and sequenced. Comparison of these sequences with the wild-type gene revealed a single sequence change for each mutant (*ar483*, T293A; *b1014*, C1816T; *ar474*, C3099T; *ar476*, G3462A; *b1018* and *ar471*, G3899A; *b1019ts* and *ar477*, G4316A; *ar511*, G4725A; *ar507*, G5594A; *b1015*, T5980A; Fig. 1g). To determine the precise coding region of *rme-6*, the apparently full-length cDNA yk629b9 was sequenced (Genbank accession number; AY750054).

Plasmids and transgenic strains

To construct *GFP::rme-6*, the *rme-6* promoter region (889bp) was PCR amplified with primers containing *Bss*H II and *Asp*718 I restriction sites and cloned into like sites in the *C. elegans* GFP vector pPD117.01 (gift of Andrew Fire). The complete coding sequence and 3′ UTR of *rme-6* (7087bp) was then PCR amplified with primers adding *Spe* I and *Apa* I restriction sites and cloned into compatible *Nhe* I and *Apa* I sites downstream of GFP in the same vector. The resulting plasmid (10 μg/ml) was co-injected with pRF4 (100 μg/ml) into N2 to establish multiple transgenic lines. Standard gamma irradiation methods were then used to attach one of these arrays to a chromosome[41] generating strain RT6: *pwIs2*. When crossed into an *rme-6 (b1014)* background, *pwIs2* fully rescued the coelomocyte endocytosis defect (Supplemental figure 3). To make *rme-6::GFP*, Gateway Reading Frame Cassette B (Invitrogen, CA) was inserted into the filled *Asp*718 I site of pPD117.01 which is located upstream of the GFP coding region. The *rme-6* gene including the promoter (864bp) and coding region without the stop codon was amplified by PCR, cloned into pDONR221, and transferred into the modified pPD117.01 by Gateway recombination cloning (Invitrogen). The resulting plasmid was introduced into *rme-6(b1014); unc-119(ed3)* by the microparticle bombardment together with a marker plasmid MM016B containing the wild-type *unc-119* gene[28]. To test rescuing activity of *rme-6::GFP*, endocytosis of microinjected Texas Red-conjugated BSA by coelomocytes was examined as described previously (Supplemental figure 3)[24].

For germline expression of transgenes, two vectors, pID3.01B and pKS1, were utilized. pID3.01B[27] drives an N-terminal GFP fusion under *pie-1* promoter control. pKS1 was made by replacing the coding sequence of GFP in pID3.01B with that of mRFP1[42]. Genomic DNA from *rme-6* and the worm clathrin heavy chain gene (*chc-1*) and a *Ce.rab-5* cDNA were cloned individually into pDONR201 and then transferred into pID3.01B or pKS1 by Gateway recombination cloning. Low copy integrated transgenic lines were obtained by the microparticle bombardment method[28]. *GFP::rme-6* under *pie-1* promoter control was directly introduced into the *rme-6(b1014)* background and examined for rescue of yolk-endocytosis.

For coelomocyte expression, pHD43 and pHD82 were used, which express N-terminal GFP and mRFP1 fusions, respectively, under the coelomocyte-specific promoter[43] (gift of H. Fares). Genomic DNA from *rme-6*, *chc-1*, worm α-*adaptin/apt-4* (T20G5.1) and worm *EEA1/eea-1* (T10G3.5) were cloned into pDONR221 and transferred into pHD43 or pHD82 by Gateway cloning. The resulting plasmids were introduced into *unc-119(ed3)* by the microparticle bombardment together with a marker plasmid MM016B. *cdEx142* [*pcc1::mRFP::rab-5*; pPD118.33] expressing *mRFP1::rab-5* under the coelomocyte-specific promoter was kindly provided by Hanna Fares (University of Arizona, AZ).

We confirmed that expression of these GFP and mRFP fusions does not interfere with endocytic function in coelomocytes and that similar results were obtained with either pair of markers, indicating that these marker fusion proteins are likely to be functional and correctly localized. The CHC-1 markers used in this study fully rescue the viability and endocytosis defects of a temperature sensitive lethal allele of *chc-1* (K. Sato and B. Grant, unpublished results).

For expression in mammalian cultured cells, an *rme-6* cDNA was cloned into pDEST53, an expression vector for N-terminal GFP fusions (Invitrogen), using the Gateway cloning system. HA-tagged *Ce.rab-5* and its mutant forms were made by PCR using a 5′-primer containing the coding sequence of the HA-tag just after the start codon. The resulting DNA fragments encoding HA-tagged RAB-5 or its mutant forms were cloned into pcDNA3.1 (Invitrogen).

Sequences of coding regions of these constructs were confirmed.

Antibodies

Anti-RME-2 anti-RME-1, and anti-EEA-1 antibodies were described previously[16,43–45]. Anti-α-adaptin antibody against the C-terminal region of *C. elegans* α-adaptin was a gift from Yinhua Zhang and David Hirsh. Anti-RME-6 polyclonal antibody was raised against the C-terminal 300 amino acids of RME-6 and affinity-purified. Ce-RABX-5 antibodies were prepared in rabbits against a synthetic peptide (CEIQAINLTSSGNQEHVEEA, corresponding to the extreme C-terminus of the protein) coupled to keyhole lympet hemocyanin, and were affinity purified against the same peptide coupled to a solid matrix (Sulfolink kit, Pierce USA) according to manufacturer's instructions. Mouse anti-HA monoclonal antibody (16B12), mouse anti-GFP monoclonal antibody (3E5) and goat anti-GFP polyclonal antibody conjugated to horse radish peroxidase (HRP) were purchased from Covance Research Products, Inc., CA, Q-BIOgene, Inc., CA and Research Diagnostics, Inc., NJ, respectively.

Microscopy, immunostaining and pulse-chase analysis in coelomocytes

Fluorescence images were obtained using an Axiovert 200M (Carl Zeiss MicroImaging, Inc., Germany) microscope equipped with a digital CCD camera (C4742-95-12ER, Hamamatsu Photonics, Japan) and Metamorph software (Universal Imaging Corp., PA) and then deconvolved with AutoDeblur software (AutoQuant Imaging Inc., NY). Confocal images were obtained using a Zeiss LSM510 confocal microscope system (Carl Zeiss MicroImaging, Inc.). Quantification of images was performed with Metamorph software (Universal Imaging Co., PA).

To observe live worms expressing transgenes, worms were mounted on agarose pads containing 10 mM levamisol in M9 buffer. Immunostaining of dissected gonad and endocytosis assays of Texas Red-conjugated BSA (TR-BSA) in coelomocytes were performed as described previously[16,24].

Immunoelectron microscopy

N2 and *rme-6(b1014)* animals were anesthetized in M9 buffer, transferred to a drop of fixative (2.8% gluteraldehyde and 2% acrolein in 0.1 M sodium cacodylate buffer) on a glass slide, and cut immediately at the level of the pharynx to facilitate penetration of fixatives. After two hours of fixation at room temperature, the animals were laid on the surface of a 10% gelatin pad where they were aligned parallel to one-another. Another drop of gelatin was then layered on top of this pad and chilled. As a result the animals were sandwiched in gelatin. Blocks were trimmed and immersed in PVP/sucrose (15%/1.7M) overnight. Ultracryomicrotomy was performed at −100C (Reichert Ultracut S/Reichert FCS, Leica, Vienna, Austria). Sections were removed from the knife with a mixture of methylcellulose/sucrose (1%/1.2M) and labeled with anti-RME2 antibody at 1:50 dilution followed by protein A conjugated with 10nm gold particles. After immunolabeling the sections were contrasted/embedded in a methylcellulose/uranylacetate mixture (1.8%/0.3%). Antibody specificity was confirmed using *rme-2(b1008)* controls.

Two-hybrid assay

The DupLEX-A two-hybrid system (OriGene Technologies, Inc., MD) was used according to manufacturer's instructions. A full length cDNA of *rme-6* was cloned into pEG202 (the bait vector). *Ce.rab-5*, *Ce.rab-7*, and their mutant forms were also cloned into pJG4-5 (the prey vector). These plasmids were introduced into reporter strains EGY48 or EGY194 included with the system. To assess the expression of the *LEU2* reporter, transformants were grown on plates lacking leucine, histidine, tryptophan and uracil, containing 2% galactose/1 % raffinose at 30°C for 3 days. Betagalactosidase assays were performed according to manufacturer's instructions.

Cell culture, transfection and immunoprecipitation

COS-7 cells were grown in Dulbecco's modified Eagle's medium/high glucose (DMEM) supplemented with 10% (v/v) fetal calf serum, 100 U/ml penicillin, 100 g/ml streptomycin and glutamine. Cells grown in 10 cm dishes were co-transfected with 5 μg of each plasmid using FuGENE 6 (Roche, IN). 48 h after transfection, cells were washed twice with ice-cold-PBS and resuspended in 1 ml of 50 mM Tris–HCl [pH 7.4], 0.5% Triton X-100, 75 mM NaCl (lysis buffer), supplemented with protease inhibitors. After a 60 min treatment at 4°C, lysates were centrifuged for 10 min at 16,000 × g at 4°C. Supernatants were incubated with protein G–Sepharose (Sigma) for 1 h and centrifuged at 16,000 × g for 10 min. Pre-cleared lysates were subsequently immunoprecipitated with anti-HA monoclonal antibody (16B12). Beads were washed twice with lysis buffer containing a reduced (0.1%) concentration of Triton X-100. Precipitants were eluted with Laemmli sample buffer and analyzed by immunoblotting using anti-GFP polyclonal antibody conjugated to HRP.

Immunoprecipitation from whole worm lysates

Transgenic worms expressing GFP::RME-6 (*pwIs2*) in the *rme-6(b1014)* background were used for coimmunoprecipitation analysis. Approximate 0.3 ml of young adults were harvested and washed with M9 buffer. They were resuspendend in 25 mM Hepes-KOH [pH7.4], 125 mM potassium acetate, 5 mM magnesium acetate, 1 mM dithiothreitol, 10% glycerol (IP buffer) containing 0.5% NP-40 and protease inhibitors and homogenized in a stainless steel homogenizer (Wheaton). Homogenates were incubated on ice for 30min and cleared by centrifugation for 5 min at 16,000 × g at 4°C. For immunoprecipitation, extracts were incubated with anti-GFP monoclonal antibody (3E6) for 1 h followed by incubation with protein A-Sepharose (Sigma) for 1 h. Beads were washed with IP buffer containing 0.1% NP-40 three times. Precipitants were subjected to immunoblotting using anti-α-adaptin and anti-EEA-1 antibodies. For a reverse experiment, α-adaptin was immunoprecipitated with anti-α-adaptin antibody from worm extracts, and precipitants were examined by immunoblotting using goat anti-GFP antibody. Control experiments using anti-GFP antibodies on N2 lysates failed to precipitate detectable α-adaptin (data not shown).

Supplementary Material

Refer to Web version on PubMed Central for supplementary material.

Acknowledgements

We thank Hanna Fares, Yinhua Zhang, David Hirsh, and Geraldine Seydoux for important reagents; Roger Y. Tsien for mRFP plasmids; Shohei Mitani for the rabx-5 knockout strain; Shigeko Yamashiro and Fumio Matsumura for help with mammalian cell culture; Iva Greenwald and Hanna Fares for critical reading of this manuscript. We also thank Peter Schweinsberg, Laura Pedraza, and Wojciech Przylecki for expert technical assistance. BG is especially grateful to David Hirsh for his strong support during the early phases of this work. MS and KS were supported by JSPS Postdoctoral Fellowship for Research Abroad and Bioarchitect Research Projects of RIKEN, respectively. This work was supported by a NIH Grant GM67237-01 and MOD Grant 5-FY02-252 to BG. BG also received support from the

Chicago Community Trust Searle Scholars Program. WL was supported by a Grant NSC 91-2320-B-182-034 of National Science Council of Taiwan.

References

1. Brodsky FM, Chen CY, Knuehl C, Towler MC, Wakeham DE. Biological basket weaving: formation and function of clathrin-coated vesicles. Annu Rev Cell Dev Biol 2001;17:517–68. [PubMed: 11687498]
2. Zerial M, McBride H. Rab proteins as membrane organizers. Nat Rev Mol Cell Biol 2001;2:107–17. [PubMed: 11252952]
3. Chavrier P, Parton RG, Hauri HP, Simons K, Zerial M. Localization of low molecular weight GTP binding proteins to exocytic and endocytic compartments. Cell 1990;62:317–29. [PubMed: 2115402]
4. Bucci C, et al. The small GTPase rab5 functions as a regulatory factor in the early endocytic pathway. Cell 1992;70:715–28. [PubMed: 1516130]
5. Christoforidis S, McBride HM, Burgoyne RD, Zerial M. The Rab5 effector EEA1 is a core component of endosome docking. Nature 1999;397:621–5. [PubMed: 10050856]
6. McBride HM, et al. Oligomeric complexes link Rab5 effectors with NSF and drive membrane fusion via interactions between EEA1 and syntaxin 13. Cell 1999;98:377–86. [PubMed: 10458612]
7. Nielsen E, Severin F, Backer JM, Hyman AA, Zerial M. Rab5 regulates motility of early endosomes on microtubules. Nat Cell Biol 1999;1:376–82. [PubMed: 10559966]
8. de Renzis S, Sonnichsen B, Zerial M. Divalent Rab effectors regulate the sub-compartmental organization and sorting of early endosomes. Nat Cell Biol 2002;4:124–33. [PubMed: 11788822]
9. Horiuchi H, et al. A novel rab5 GDP/GTP exchange factor complexed to rabaptin-5 links nucleotide exchange to effector recruitment and function. Cell 1997;90:1149–1159. [PubMed: 9323142]
10. Rubino M, Miaczynska M, Lippe R, Zerial M. Selective membrane recruitment of EEA1 suggests a role in directional transport of clathrin-coated vesicles to early endosomes. J Biol Chem 2000;275:3745–8. [PubMed: 10660521]
11. McLauchlan H, et al. A novel role for Rab5-GDI in ligand sequestration into clathrin-coated pits. Curr Biol 1998;8:34–45. [PubMed: 9427626]
12. Delprato A, Merithew E, Lambright DG. Structure, exchange determinants, and family-wide rab specificity of the tandem helical bundle and Vps9 domains of Rabex-5. Cell 2004;118:607–17. [PubMed: 15339665]
13. Tall GG, Barbieri MA, Stahl PD, Horazdovsky BF. Ras-activated endocytosis is mediated by the Rab5 guanine nucleotide exchange activity of RIN1. Dev Cell 2001;1:73–82. [PubMed: 11703925]
14. Topp JD, Gray NW, Gerard RD, Horazdovsky BF. Alsin is a Rab5 and Rac1 guanine nucleotide exchange factor. J Biol Chem 2004;279:24612–23. [PubMed: 15033976]
15. Horiuchi H, Giner A, Hoflack B, Zerial M. A GDP/GTP exchange-stimulatory activity for the Rab5-RabGDI complex on clathrin-coated vesicles from bovine brain. J Biol Chem 1995;270:11257–62. [PubMed: 7744760]
16. Grant B, Hirsh D. Receptor-mediated endocytosis in the Caenorhabditis elegans oocyte. Mol Biol Cell 1999;10:4311–26. [PubMed: 10588660]
17. Fares H, Greenwald I. Genetic analysis of endocytosis in Caenorhabditis elegans: coelomocyte uptake defective mutants. Genetics 2001;159:133–45. [PubMed: 11560892]
18. Bernards A. GAPs galore! A survey of putative Ras superfamily GTPase activating proteins in man and Drosophila. Biochim Biophys Acta 2003;1603:47–82. [PubMed: 12618308]
19. Hajnal A, Whitfield CW, Kim SK. Inhibition of Caenorhabditis elegans vulval induction by gap-1 and by let-23 receptor tyrosine kinase. Genes Dev 1997;11:2715–28. [PubMed: 9334333]
20. Hayashizaki S, Iino Y, Yamamoto M. Characterization of the C. elegans gap-2 gene encoding a novel Ras-GTPase activating protein and its possible role in larval development. Genes Cells 1998;3:189–202. [PubMed: 9619631]
21. Hart MJ, Callow MG, Souza B, Polakis P. IQGAP1, a calmodulin-binding protein with a rasGAP-related domain, is a potential effector for cdc42Hs. Embo J 1996;15:2997–3005. [PubMed: 8670801]
22. Hama H, Tall GG, Horazdovsky BF. Vps9p is a guanine nucleotide exchange factor involved in vesicle-mediated vacuolar protein transport. J Biol Chem 1999;274:15284–91. [PubMed: 10329739]

23. Stenmark H, Vitale G, Ullrich O, Zerial M. Rabaptin-5 is a direct effector of the small GTPase Rab5 in endocytic membrane fusion. Cell 1995;83:423–32. [PubMed: 8521472]
24. Zhang Y, Grant B, Hirsh D. RME-8, a conserved J-domain protein, is required for endocytosis in Caenorhabditis elegans. Mol Biol Cell 2001;12:2011–21. [PubMed: 11451999]
25. Greener T, et al. Caenorhabditis elegans auxilin: a J-domain protein essential for clathrin-mediated endocytosis in vivo. Nat Cell Biol 2001;3:215–9. [PubMed: 11175756]
26. Fares H, Grant B. Deciphering endocytosis in Caenorhabditis elegans. Traffic 2002;3:11–9. [PubMed: 11872138]
27. Pellettieri J, Reinke V, Kim SK, Seydoux G. Coordinate activation of maternal protein degradation during the egg-to-embryo transition in C. elegans. Dev Cell 2003;5:451–62. [PubMed: 12967564]
28. Praitis V, Casey E, Collar D, Austin J. Creation of low-copy integrated transgenic lines in Caenorhabditis elegans. Genetics 2001;157:1217–26. [PubMed: 11238406]
29. Barbieri MA, et al. Epidermal growth factor and membrane trafficking. EGF receptor activation of endocytosis requires Rab5a. J Cell Biol 2000;151:539–50. [PubMed: 11062256]
30. Galperin E, Sorkin A. Visualization of Rab5 activity in living cells by FRET microscopy and influence of plasma-membrane-targeted Rab5 on clathrin-dependent endocytosis. J Cell Sci 2003;116:4799–810. [PubMed: 14600265]
31. Christoforidis S, et al. Phosphatidylinositol-3-OH kinases are Rab5 effectors. Nat Cell Biol 1999;1:249–52. [PubMed: 10559924]
32. Shiba Y, Takatsu H, Shin HW, Nakayama K. Gamma-adaptin interacts directly with Rabaptin-5 through its ear domain. J Biochem (Tokyo) 2002;131:327–36. [PubMed: 11872161]
33. Mattera R, Arighi CN, Lodge R, Zerial M, Bonifacino JS. Divalent interaction of the GGAs with the Rabaptin-5-Rabex-5 complex. Embo J 2003;22:78–88. [PubMed: 12505986]
34. Mishra SK, et al. Dual-engagement regulation of protein interactions with the AP-2 adaptor alpha appendage. J Biol Chem. 2004
35. Han M, Sternberg PW. let-60, a gene that specifies cell fates during C. elegans vulval induction, encodes a ras protein. Cell 1990;63:921–31. [PubMed: 2257629]
36. Brenner S. The genetics of Caenorhabditis elegans. Genetics 1974;77:71–94. [PubMed: 4366476]
37. Dang H, Li Z, Skolnik EY, Fares H. Disease-related myotubularins function in endocytic traffic in Caenorhabditis elegans. Mol Biol Cell 2004;15:189–96. [PubMed: 14565969]
38. Kamath RS, Ahringer J. Genome-wide RNAi screening in Caenorhabditis elegans. Methods 2003;30:313–21. [PubMed: 12828945]
39. Timmons L, Court DL, Fire A. Ingestion of bacterially expressed dsRNAs can produce specific and potent genetic interference in Caenorhabditis elegans. Gene 2001;263:103–12. [PubMed: 11223248]
40. Williams BD, Schrank B, Huynh C, Shownkeen R, Waterston RH. A genetic mapping system in Caenorhabditis elegans based on polymorphic sequence-tagged sites. Genetics 1992;131:609–24. [PubMed: 1321065]
41. Mello CC, Kramer JM, Stinchcomb D, Ambros V. Efficient gene transfer in C.elegans: extrachromosomal maintenance and integration of transforming sequences. Embo J 1991;10:3959–70. [PubMed: 1935914]
42. Campbell RE, et al. A monomeric red fluorescent protein. Proc Natl Acad Sci U S A 2002;99:7877–82. [PubMed: 12060735]
43. Fares H, Greenwald I. Regulation of endocytosis by CUP-5, the Caenorhabditis elegans mucolipin-1 homolog. Nat Genet 2001;28:64–8. [PubMed: 11326278]
44. Grant B, et al. Evidence that RME-1, a conserved C. elegans EH-domain protein, functions in endocytic recycling. Nat Cell Biol 2001;3:573–9. [PubMed: 11389442]
45. Shaye DD, Greenwald I. Endocytosis-mediated downregulation of LIN-12/Notch upon Ras activation in Caenorhabditis elegans. Nature 2002;420:686–90. [PubMed: 12478297]

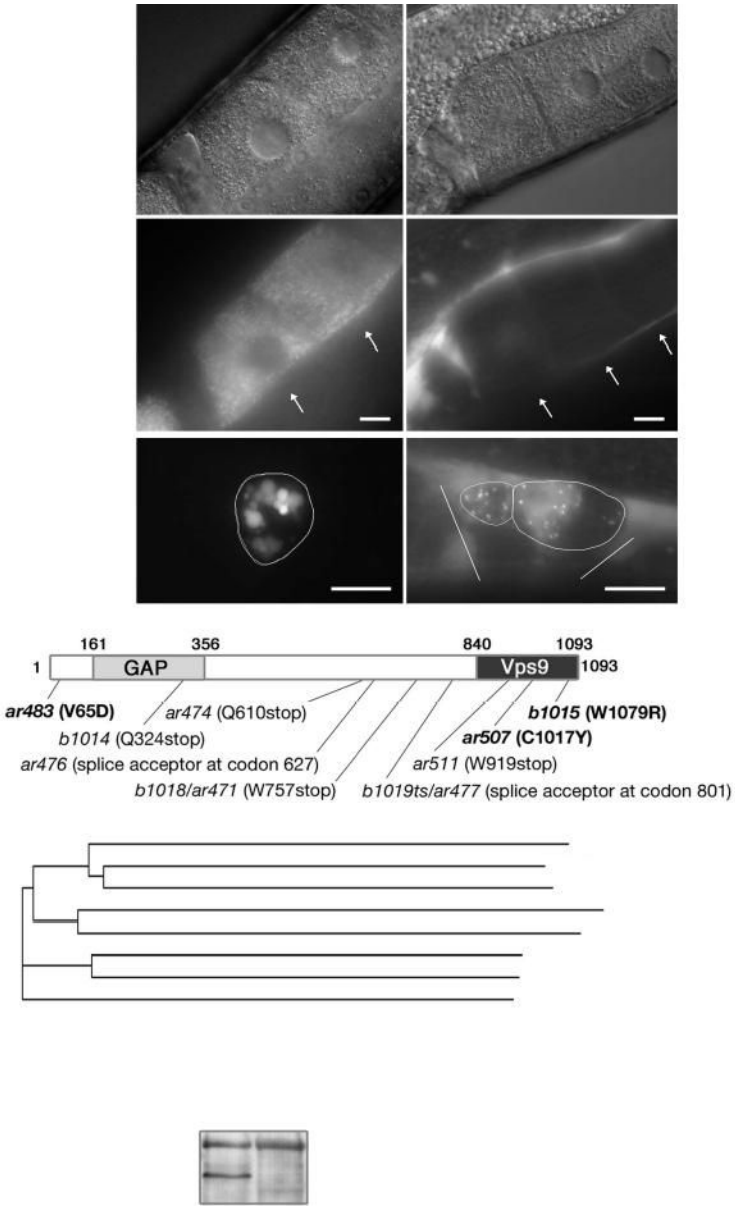

Figure 1.

rme-6 mutant phenotypes and diagram of the predicted RME-6 protein. (a–d) YP170::GFP endocytosis by oocytes of adult hermaphrodites. In wild-type, YP170::GFP is efficiently endocytosed by oocytes (c). In the *rme-6(b1014)* mutant, endocytosis of YP170::GFP by oocytes is greatly reduced and most YP170::GFP accumulates in the body cavity (d). Nomarski images of the same fields are also shown in a and b. Arrows indicate the position of oocytes. SP, spermatheca. (e and f) Coelomocyte endocytosis assay using GFP secreted from body-wall muscle cells. Secreted GFP is taken up by coelomocytes and accumulates in vesicles of wild-type coelomocytes (e). In *rme-6(ar507)* strong accumulation of GFP in the body cavity was observed indicating poor endocytosis by coelomocytes (f). Some secreted GFP does accumulate within the coelomocytes of *rme-6* mutants, but the vesicles labeled by the internalized GFP are abnormally small (see Results). Cell boundaries of coelomocytes are outlined for clarity. Bar, 10 μm. (g) Domain structure of RME-6, showing the N-terminal RasGAP-related domain and the Vps9 domain at the C-terminus. Mutations identified in each

of the 11 *rme-6* alleles are also shown, including three missense mutations shown in bold. Nucleotide sequence changes in *rme-6* mutants: *ar483*(T293A), *b1014*(C1816T), *ar474* (C3099T), *ar476*(G3462A), *b1018/ar471*(G3899A), *b1019ts/ar477*(G4316A), *ar511 (*G4725A), *ar507(*G5594A), *b1015(*T5980A). (h) Phylogenic analysis of Vps9 domain proteins. Amino acid sequences of indicated proteins were analysed by ClustalW. Ce, *C. elegans*; Hs, *Homo sapiens*; Dm, *Drosophila melanogaster*; Sc, *Saccharomyces cerevisiae*. (i) Detection of RME-6 protein. Total lysates were prepared from wild-type and *rme-6(b1014)* mutant worm and examined by immunoblotting using anti-RME-6 antibodies. Asterisk indicates a nonspecific band.

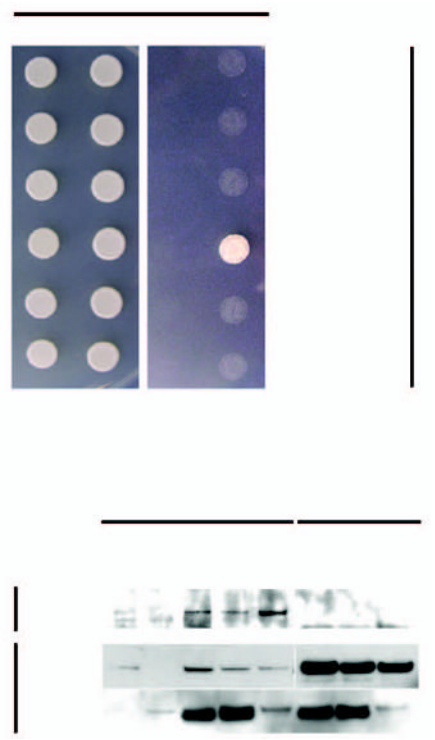

Figure 2.

RME-6 physically interacts with RAB-5(S33N). (a) Two-hybrid assay between RME-6 and RAB-5. Full length RME-6 was expressed in a yeast reporter strain as a fusion with the DNA binding domain of LexA (bait). Full length *C. elegans* RAB-5, RAB-*7* and their mutant forms were expressed in the same yeast cells as fusions with the transcriptional activation domain of B42 (prey). Interaction between bait and prey was tested using *LEU2* (shown) and beta-galactosidase (not shown) reporter assays. (b) Co-immunoprecipitation of GFP::RME-6 and HA-RAB-5 or their mutant forms co-expressed in COS-7 cells. HA-RAB-5 was immunoprecipitated with anti-HA antibody and precipitants were analyzed by immunoblotting using anti-GFP antibody. Aliquots of total cell lysates were also examined by immunoblotting using anti-HA and anti-GFP antibodies.

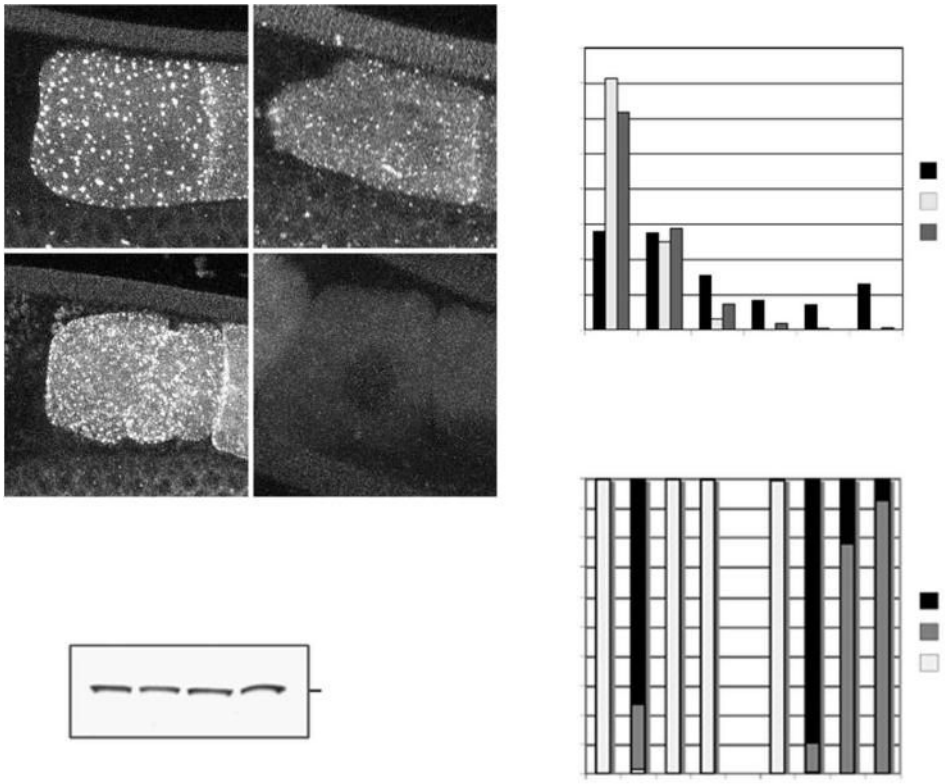

Figure 3.

rme-6 and *rabx-5* function in membrane recruitment of GFP::RAB-5 and animal viability. (a–d) Subcellular localization of GFP::RAB-5 in oocytes was observed in wild-type (a), *rme-6 (b1014)* (b), *rabx-5(RNAi)* (c) and *rme-6(b1014); rabx-5(RNAi)* worms (d). Oocytes were optically sectioned by confocal microscopy. Projected images of confocal z-stacks are shown. (e) Detection of GFP::RAB-5 by immunoblotting using an anti-GFP antibody. The protein level of GFP::RAB-5 was not affected by *rme-6(b1014)* nor *rabx-5(RNAi)*. (f) Size distribution of GFP::RAB-5-positive endosomes in wild-type, *rme-6(b1014)*, and *rabx-5(RNAi)* backgrounds. In each case quantification of GFP::RAB-5 puncta was performed on oocytes closest to the spermatheca. (g) The phenotypic effects of RNAi-based gene knockdown of *rab-5*, *rabx-5*, or *rabn-5* in wild-type or *rme-6* mutant backgrounds were assayed. L4 larvae were placed on RNAi plates and phenotype of FI progeny was scored.

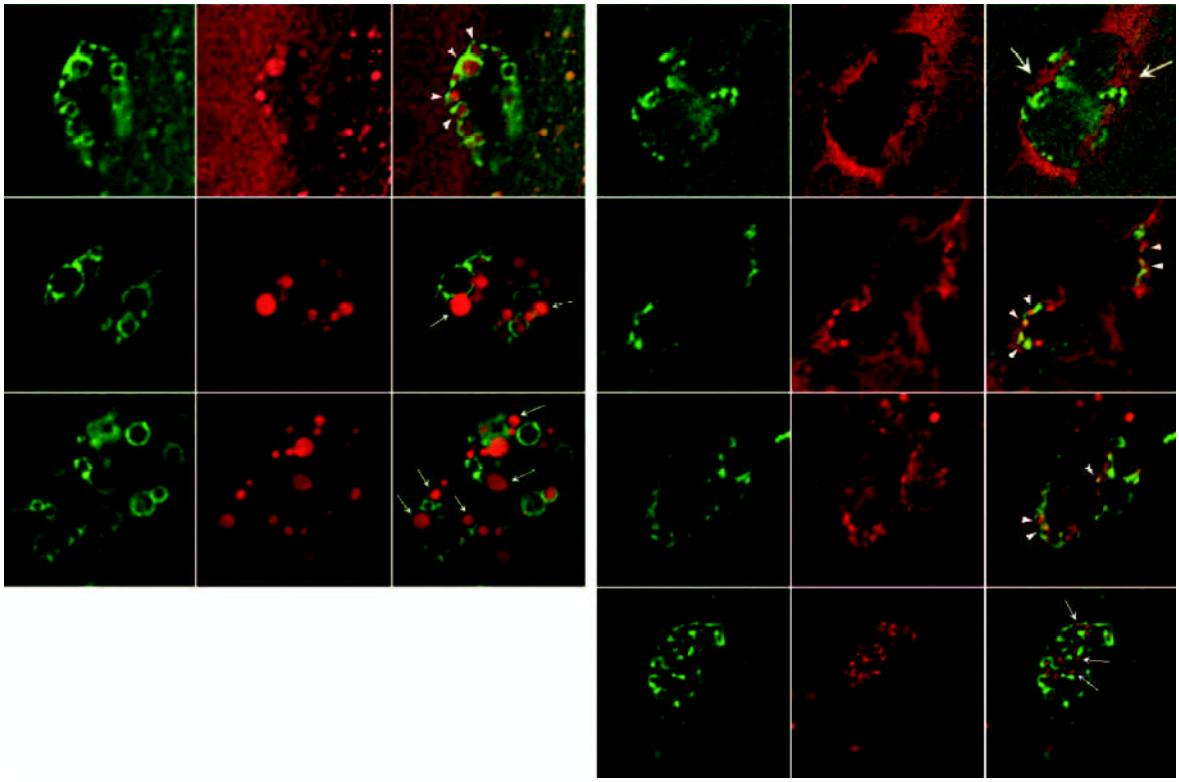

Figure 4.

An early stage of endocytosis is slowed in *rme-6* mutant coelomocytes. (a) TR-BSA was microinjected into the body cavity, and endocytic trafficking of TR-BSA in coelomocytes was observed at different time points after injection. To visualize endosomes within coelomocytes, transgenic worms expressing RME-8::GFP were used. In wild-type, TR-BSA first appeared inside RME-8::GFP-positive endosomes 5 to 10 min after injection (arrow heads). After 30 min, TR-BSA began to accumulate in the RME-8::GFP-negative lysosomes (small arrows). (b) The same time-course of TR-BSA uptake by coelomocytes was analyzed in *rme-6 (b1014)* mutants expressing the RME-8::GFP endosome marker. At early time points, TR-BSA showed a diffuse pattern close to the PM (large arrows). Significant overlap between TR-BSA and RME-8::GFP signals was observed during the 30 and 60 min timepoints (arrow heads). Finally, TR-BSA accumulated in RME-8::GFP negative compartments 120 min after injection (small arrows).

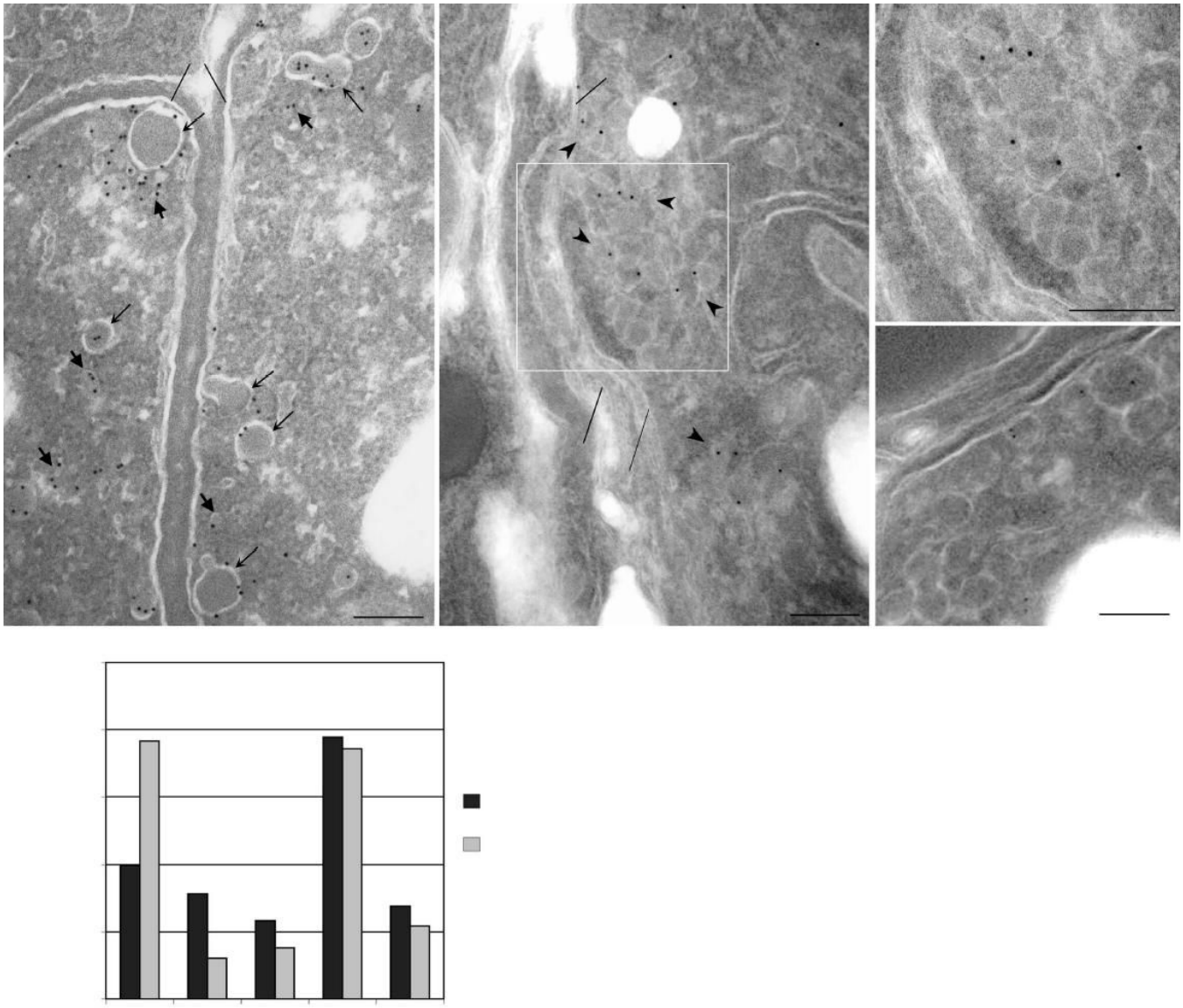

Figure 5.

rme-6 accumulates chains of small yolk receptor positive vesicles. Immunoelectron microscopy of endogenous yolk receptors (RME-2) was performed in wild-type (a) and *rme-6 (b1014)* mutants (b–d). RME-2 localizes to the PM, cortical electron transparent vesicles (large arrows) and larger more electron dense vesicles (small arrows) in wild-type oocytes (see results). In *rme-6* mutants, RME-2 yolk receptors are observed on grape-like chains of small vesicles (arrow heads). Images of *rme-6* mutants at high-magnification are shown in panel c (a part of b) and d (a different field). Bar, 200 nm. (e) Quantitative analysis of RME-2 distribution. RME-2 positive structures were classified as vesicles smaller or larger than 120 nm in diameter, PM or tubulo-vesicular structures. The number of particles associated with these structures was counted in wild-type (823 particles in total) and *rme-6* mutant (773 particles in total) oocytes.

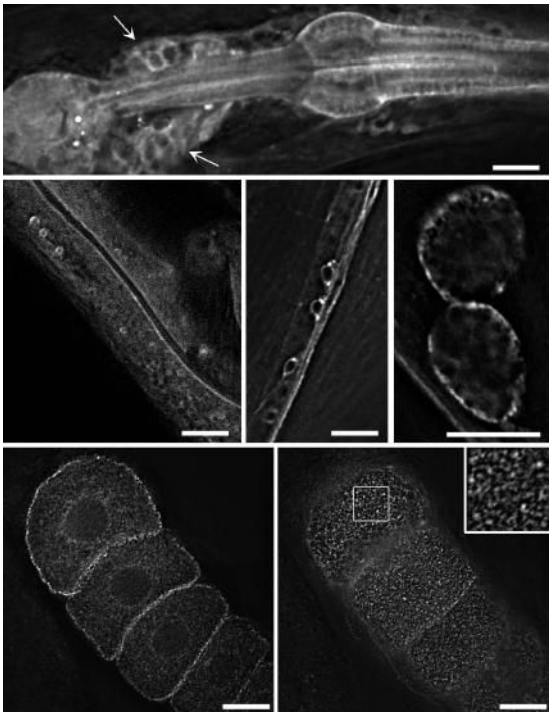

Figure 6.

Expression and subcellular localization of GFP::RME-6 in worm tissues. (a–d) Expression of a rescuing GFP::RME-6 fusion in live animals under *rme-6* promoter control. Expression was observed in pharynx (a), intestine (b), neurons (arrows in a and c) and coelomocytes (d). (e and f) A rescuing GFP::RME-6 fusion expressed in oocytes under *pie-1* promoter control. Dissected gonads of the transgenic worms were stained with an anti-GFP monoclonal antibody. GFP::RME-6 is enriched in cortical puncta of oocytes. Middle (e) and surface (f) of oocytes are shown. Bar, 10 μm.

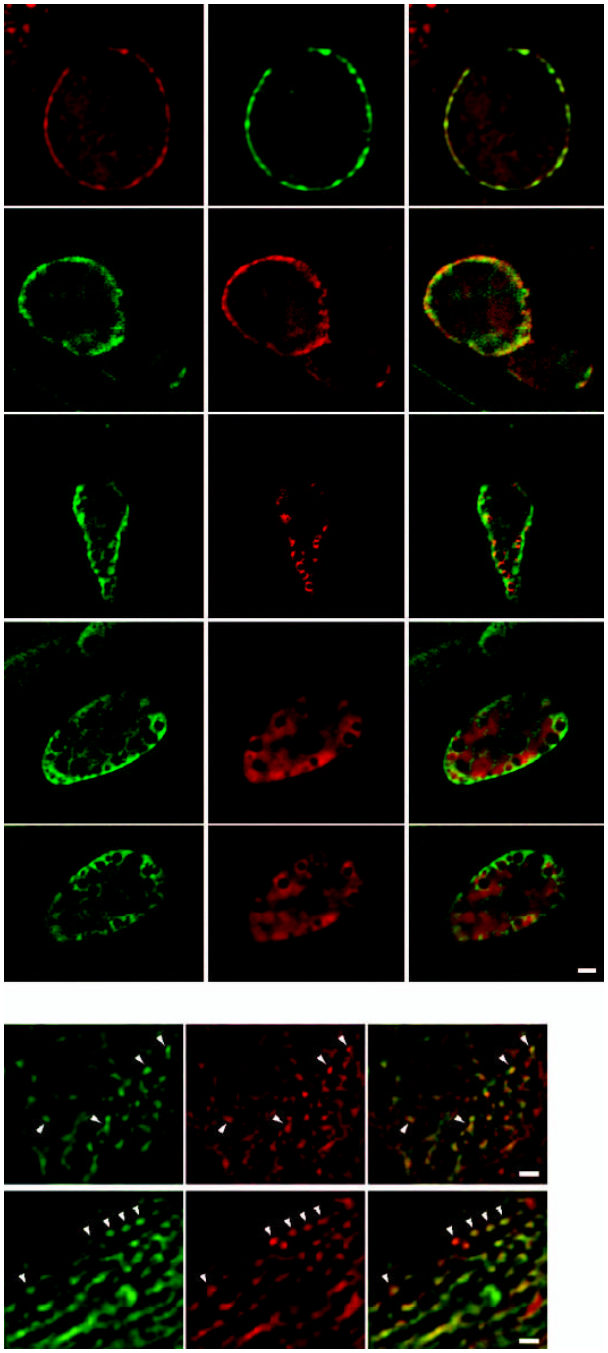

Figure 7.
GFP::RME-6 colocalizes strongly with clathrin-coated pit markers. (a) Colocalization of mRFP::RME-6 and GFP::CHC-1 in coelomocytes. (b–d) Subcellular localization of GFP::RME-6 and organeller markers in coelomocytes. GFP::RME-6 and the indicated mRFP1 fusions were co-expressed in coelomocytes. Strong colocalization was observed between GFP::RME-6 and α-adaptin/APT-4 (b). GFP::RME-6 only weakly colocalized with early endosome markers mRFP::EEA-1 (c) and mRFP::RAB-5 (d). (e and f) Co-localization of GFP::RME-6 and mRFP1::CHC-1 in the cortex of oocytes (e) and hypodermal cells (f) in an *rme-6(b1014)* background. Bar, 2 μm.

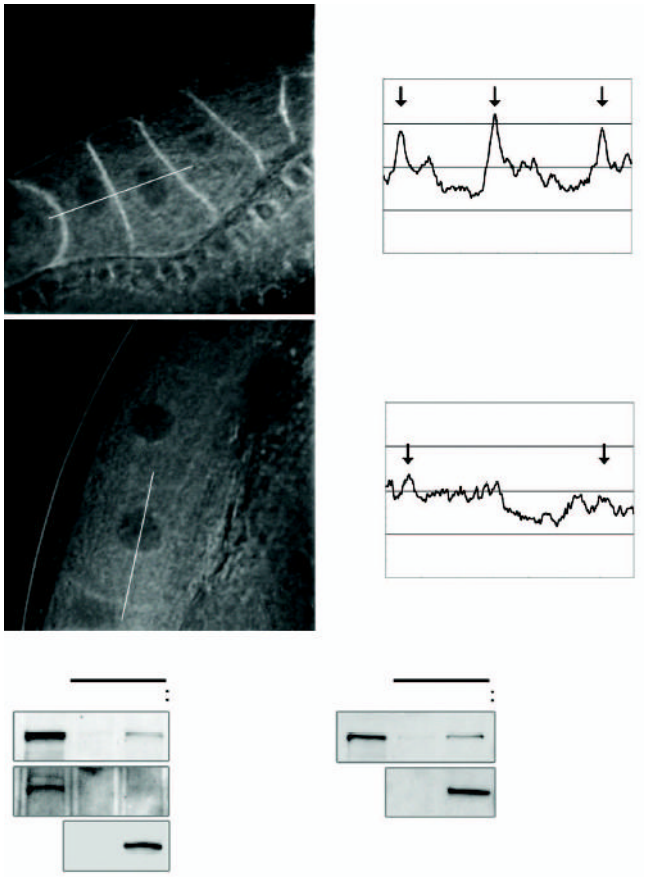

Figure 8.

(a–d) RNAi-mediated knockdown of clathrin heavy chain but not *rab-5* disrupts the cortical localization of GFP::RME-6 in oocytes. RNAi of *rab-5* (a) or *chc-1* (b) was performed in worms expressing GFP::RME-6 in oocytes. P_0 worms grown on RNAi bacteria for 24 h at 25° C. Fluorescence intensity as a function of position was graphed using Metamorph software along the lines indicated in panel a (c) and b (d). Arrows indicate the relative position of oocyte plasma membranes. (e and f) GFP::RME-6 and α-adaptin co-immunoprecipitate from whole worm lysates. Total lysates were prepared from worms expressing GFP::RME-6 in an *rme-6 (b1014)* background and subjected to immunoprecipitation with anti-GFP antibody (e) or anti-α-adaptin antibody (f). Precipitants were probed on Western blots with anti-α-adaptin and anti-EEA-1 antibodies (e) or anti-GFP antibody (f). T (total lysate) equals approximately 1.5% of the total input into the assay.